Effect of grain size sorting on the formation of shoreface-connected sand ridges

M. Walgreen and H. E. de Swart
Institute for Marine and Atmospheric Research (IMAU), Utrecht University, Utrecht, Netherlands

D. Calvete
Department de Física Applicada, Universitat Politècnica de Catalunya, Barcelona, Spain

Received 11 April 2002; revised 29 November 2002; accepted 6 December 2002; published 6 March 2003.

[1] Field data of shoreface-connected ridges show persistent spatial variations of mean grain size over the bed forms. In the shore-normal direction, the profiles of bottom topography and mean grain size are approximately 90° out of phase. To investigate the mechanisms responsible for the observed grain size distribution and the influence of sediment sorting on the temporal and spatial characteristics of shoreface-connected ridges, a model is developed and analyzed. A linear stability analysis of an alongshore uniform basic state (describing a storm-driven flow on a microtidal inner shelf) with respect to small bottom perturbations is carried out. The transport of nonuniform sediment is described by formulations for both bed load and suspended load, both of which account for dynamic hiding effects. A one-layer model for the bed evolution and a bottom friction term, which depends on the grain size, are used. The initial formation of the ridges is studied for a bimodal sediment mixture. The results of the model indicate that the phase shift between bed topography and mean grain size for shoreface-connected ridges is due to the selective transport via suspended load of grains with different sizes. A net stabilizing effect on the growth of bed forms and enhanced migration are predicted, caused by the bimodal character of the sediment. The wavelengths of the bed forms are only slightly affected. Including a tidal current or a grain size dependent formulation for the bottom friction has no effect on the results. A physical explanation for the model results is also given. *INDEX TERMS:* 3022 Marine Geology and Geophysics: Marine sediments—processes and transport; 4219 Oceanography: General: Continental shelf processes; 4255 Oceanography: General: Numerical modeling; 4558 Oceanography: Physical: Sediment transport; 4512 Oceanography: Physical: Currents; *KEYWORDS:* morphodynamic model, shoreface-connected ridges, grain sorting, hiding, sediment transport, nonuniform sediment

Citation: Walgreen, M., H. E. de Swart, and D. Calvete, Effect of grain size sorting on the formation of shoreface-connected sand ridges, *J. Geophys. Res.*, *108*(C3), 3063, doi:10.1029/2002JC001435, 2003.

1. Introduction

[2] Shoreface-connected ridges are rhythmic bed forms that are observed on storm-dominated inner shelves of coastal seas, in water depths of 4–20 m. Analysis of field observations [*Swift et al.*, 1978; *Antia*, 1996; *Van de Meene and Van Rijn*, 2000] has revealed that the spacing between the crests is in the order of 5–10 km, with heights varying between 1 and 6 m. Migration occurs in the direction of the mean alongshore storm-driven flow, and characteristic phase speeds are 1–4 m yr^{-1}. Previous model studies have demonstrated that the formation of these large-scale bed forms is due to inherent positive feedbacks between the water motion and the eroding bed [*Trowbridge*, 1995; *Calvete et al.*, 2001a, 2001b]. The combined action of stirring of sediment by waves and transport by storm-driven currents is necessary to generate shoreface-connected ridges. Furthermore, these studies have found that the seaward end of the ridges is always shifted upcurrent with respect to their attachments to the shoreface and explanations for this morphological characteristic have been put forward. The model developed by *Calvete et al.* [2001b] provides information on the spatial pattern, evolution timescale and migration speed of the bed forms. These results are in good agreement with available field data of many different shelves.

[3] A basic limitation of these models is that they assume a uniform grain size distribution of the sediment. This is not consistent with field data, which show persistent spatial variations of the mean grain size over the bed forms. Especially the ridges on the Mid-Atlantic shelf are documented extensively and detailed information on the grain size characteristics has been given in the literature [see, for example, *Swift et al.*, 1972; *Hoogendoorn*, 1986; *Schwab et al.*, 2000]. The ridges located in the Mid-Atlantic Bight on the North American inner shelf [*Swift et al.*, 1978; *Swift and Field*, 1981; *Figueiredo et al.*, 1982] reveal, in the direction normal to the shore, grain size and topography variations that

0148-0227/03/2002JC001435$09.00

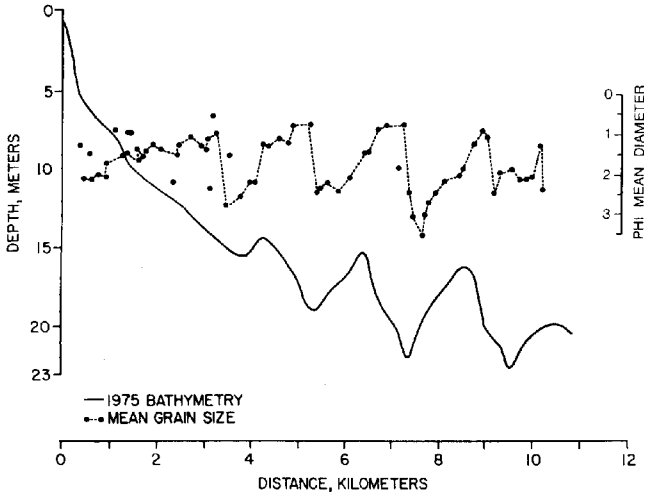

Figure 1. Measured shore-normal profile of water depth (in meters) and mean grain size (in phi units) for the shoreface-connected ridges on the Long Island inner shelf. Larger phi values imply smaller grain sizes. From *Figueiredo et al.* [1982], ©Elsevier Science.

are approximately 90° out of phase: the coarsest material occurs on the landward (upcurrent) flank. This out-of-phase relationship extends over the entire ridge area (Figure 1). The mean diameter as plotted here is defined in section 2.2. Similar trends in mean grain size are observed for shoreface-connected ridges on the inner shelf of Brazil [*Figueiredo et al.*, 1982] and Argentina [*Parker et al.*, 1982], and for similar ridges located in the German Bight of the southern North Sea [*Antia*, 1996].

[4] In the present study, the effect of sediment sorting on the formation of shoreface-connected ridges is investigated by extending the model by *Calvete et al.* [2001b] for sediment mixtures. New dynamics related to the presence of different grain sizes are incorporated in the sediment transport formulation, the sediment continuity equation, and in the formulation of the bottom friction in the hydrodynamic equations. Previous model studies on sediment sorting have mainly focused on river bars and sea ripples [*Ribberink*, 1987; *Seminara*, 1995; *Foti and Blondeaux*, 1995; *Lanzoni and Tubino*, 1999], i.e., on spatial scales much smaller than those for sand ridges. These studies indicate that the nonuniform character of sediment has a stabilizing effect on the growth of bed forms.

[5] The work presented in this paper contains several new aspects. First, it focuses on sediment sorting in the sand fraction in combination with ridge formation, while previous work has largely concentrated on gravel and sand–gravel mixtures (representative of river sediments). Second, the influence of grain size on the entrainment and deposition of suspended sediment is included. Third, the effect of sediment sorting in the modeling of large-scale bed forms in coastal seas is investigated. The first objective of this paper was to investigate the influence of sediment sorting on the temporal and spatial characteristics of shoreface-connected ridges. The second goal was to gain insight into the physical mechanisms responsible for the observed grain size distribution over shoreface-connected ridges. This paper focuses on the initial formation of shoreface-connected ridges, i.e., small bottom perturbations are assumed. Therefore, a one-layer model for the bottom evolution, based on the concept of an active transport layer overlaying an inactive substrate, is used. The model uses a two-size sediment mixture. The motivation for using a simple model is that it allows for a systematic analysis of the underlying processes.

[6] In section 2, the formulation of the model is given, followed by an outline of the solution procedure in section 3. Results are presented in section 4 and a physical interpretation is given in section 5. A discussion of the model results, including a comparison with field observations, is presented in section 6, followed by conclusions in the last section.

2. Model Formulation

2.1. Hydrodynamics

[7] Following earlier studies by *Trowbridge* [1995] and *Calvete et al.* [2001b], we hypothesize that shoreface-connected sand ridges form as an inherent instability of a morphodynamic system, in which there is a feedback between the storm-driven flow and the eroding bed. A highly idealized model is used to investigate the flow–topography interaction on coastal shelves during storm conditions. The shelf geometry is schematized as a semi-infinite domain, bounded on the landward side by the transition from the shoreface to the inner shelf (see Figure 2). The undisturbed bathymetry (no ridges present) is uniform in the alongshore (y) direction. In the cross-shore (x) direction it consists of an inner shelf (with a linearly sloping bottom) and an outer shelf represented by a horizontal bottom. The water depth at the beginning of the inner shelf ($x = 0$) is H_0, L_s is the inner shelf width and H_s is the depth of the outer shelf. Representative values for the Long Island inner shelf (Mid-Atlantic Bight, US), which is considered as a prototype storm-driven shelf in this study, are $H_0 = 14$ m, $H_s = 20$ m and $L_s = 5.5$ km.

[8] In the model the water motion is described by the 2DH shallow water equations. They read

$$\frac{\partial \vec{v}}{\partial t} + \left(\vec{v}\cdot\vec{\nabla}\right)\vec{v} + \vec{f}\times\vec{v} = -g\vec{\nabla}z_s + \frac{\vec{\tau}_s - \vec{\tau}_b}{\rho D} \tag{1}$$

$$\frac{\partial D}{\partial t} + \vec{\nabla}\cdot(D\vec{v}) = 0 \tag{2}$$

Here $\vec{v}$ is the depth-averaged and wave-averaged velocity, $f \sim 10^{-4}$ s^{-1} is the Coriolis parameter, $\vec{\tau}_s$ the wind shear stress vector, $\vec{\tau}_b$ the bottom shear stress vector, g the

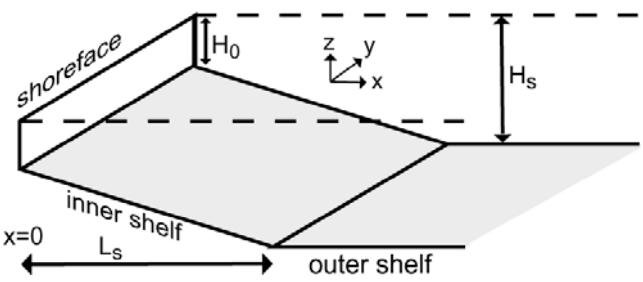

Figure 2. Sketch of the geometry of the model, representing the inner shelf (width L_s) and part of the outer shelf of a coastal sea. For further information, see the text.

acceleration due to gravity, ρ the density of water, t the time and $\vec{\nabla}$ the horizontal nabla operator. The local water depth is given by $D = z_s - z_b$, where z_s is the free surface elevation and z_b is the bottom depth, both measured with respect to the undisturbed water level $z = 0$.

[9] Both observations and model studies indicate that shoreface-connected ridges mainly develop during storms, tides do not play an important role, and the timescales involved are about 100 years. This appears to justify the neglect of tidal forcing in the model (microtidal shelves are assumed) and the use of a probabilistic approach. Two realizations of the system are considered. During storms (which occur during a time fraction $\mu \sim 0.05$) large waves and strong currents cause significant sediment transport. In contrast, during fair weather conditions (time fraction $1 - \mu$) the waves and currents are not sufficiently strong to erode sediment from the bottom. Thus, (1) and (2) are assumed to be representative of conditions during storms. The quasi-steady approximation is made in (1) and (2), such that terms involving time derivatives are excluded. This is because the hydrodynamic timescale is much smaller than the timescale on which the bed evolves. Also, the rigid-lid assumption is used, in which case the free surface effects in the local water depth are neglected, i.e., $D \simeq -z_b$.

[10] The main forcing of the water motion is by wind and an alongshore pressure gradient. During storms the presence of large waves causes a wave-orbital velocity amplitude u_w, which is much larger than the wave-averaged velocity amplitude. This allows for a linearization of the bed shear stress:

$$\vec{\tau}_b = \rho r \vec{v}$$

with r the bottom friction coefficient which is written in terms of a Chezy coefficient C_h [see *Ribberink*, 1987; *Soulsby*, 1997]. This results in

$$r = \frac{g\langle|\hat{u}_w|\rangle}{C_h^2} \quad C_h = \frac{\sqrt{g}}{\kappa}\ln\left(\frac{12D}{k_s}\right) \tag{3}$$

where $\hat{u}_w$ is the near-bed wave-orbital velocity and $\langle\ldots\rangle$ denotes a time average over many wave periods. Furthermore, κ is the von Karman's constant and k_s is the roughness length, which is proportional to a coarse grain size [see, for example, *Ribberink*, 1987; *Lanzoni and Tubino*, 1999]. This formulation of the friction coefficient introduces a dependence on the grain size in the hydrodynamic equations. The value we used for the friction coefficient is $r \sim 7 \times 10^{-4}$ m s^{-1}.

[11] *Calvete et al.* [2001b] found that it is essential for the growth of shoreface-connected ridges to parameterize the wave-orbital velocity increase in decreasing water depths. The description of the wave-orbital velocity as $\hat{u}_w = u_w \cos(\omega t)$ (symmetrical waves with frequency ω), with the amplitude given by

$$u_w = U_w(H_0/H)^{\frac{m}{2}}, \tag{4}$$

includes this effect. Here H is the undisturbed water depth, $U_w \sim 1$ m s^{-1} the amplitude at the shoreface boundary $x = 0$ and m a coefficient. Runs with a simple wave shoaling model indicate that $m \sim 1.6$.

2.2. Sediment Characteristics

[12] For a sediment mixture it is convenient to use a logarithmic scale (the phi scale) to describe the grain diameters. The definition is

$$d = 2^{-\phi} \quad \text{or} \quad \phi = -\log_2 d$$

where d is the grain diameter measured in units of mm [see *Dyer*, 1986]. Accordingly, larger values of ϕ correspond to finer sizes. A sediment mixture is described by a probability distribution function $\mathcal{F}$ as a function of the grain size. This is the weight percentage of each grain size, hence $\mathcal{F}$ has the following property:

$$\int_{-\infty}^{\infty} \mathcal{F}(\phi)d\phi = 1$$

For many sand mixtures $\mathcal{F}(\phi)$ is approximately a Gaussian curve if plotted on this phi scale. In that case, two statistical properties describe the sediment distribution: the mean grain diameter ϕ_m and the standard deviation σ, defined as

$$\phi_m = \int_{-\infty}^{\infty} \phi\mathcal{F}(\phi)d\phi \quad \sigma^2 = \int_{-\infty}^{\infty} (\phi - \phi_m)^2\mathcal{F}(\phi)d\phi$$

The mean diameter is calculated as $d_m = 2^{-\phi_m}$. A measure of the sorting is given by the standard deviation of the distribution. Small values of σ corresponds to a sharply peaked curve, representing an almost uniform sample, and is classified as well sorted. A poorly sorted mixture of sediment has larger values of σ.

2.3. Sediment Continuity

[13] The hydrodynamic equations discussed above are supplemented with a sediment transport formulation, based on the concepts introduced by *Bailard* [1981] for the total load transport on a sloping bed, and the bottom evolution equation. The evolution of the bottom is a result of divergence in the sediment flux and depends on the composition of the bottom sediment. The simplest models dealing with the effect of sediment sorting on bed level changes consider two separate layers in the bottom (Figure 3) [see *Ribberink*, 1987; *Seminara*, 1995]. The first is the active layer, which contains the material available for transport, and $\mathcal{F}$ is the corresponding probability density function for the grain sizes in this layer. Underneath this active layer a substrate is located with a probability density function of $\mathcal{F}_s$. The bottom location is denoted by $z_b = -H + h$, with H the undisturbed water depth and h the bed elevation with respect to this reference level. Furthermore, $z_\eta = z_b - L_a$ is the level of the interface between the active (surface) layer and the substrate. The active layer thickness, L_a, is in the order of 2–3 times d_{90} (grain size for which 90% of the material is finer). The thickness of the total sediment column is considered to be so large that modifications of the sediment composition in the substrate, due to exchanges of sediment with the upper layer, can be omitted.

[14] A well-mixed active layer ($\mathcal{F}$ is independent of the depth) and a time-independent grain size composition in the

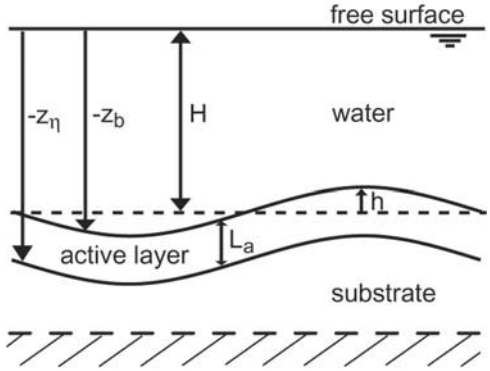

Figure 3. Definition of the sediment layer as used in the model. The thickness of the active layer is denoted by L_a, and h is the elevation of the bottom with respect to a reference level.

substrate ($\mathcal{F}_s$) were assumed. Consequently, the continuity equation of sediment reads

$$\mathcal{F}_\eta \frac{\partial h}{\partial t} + L_a \frac{\partial \mathcal{F}}{\partial t} + (\mathcal{F} - \mathcal{F}_\eta)\frac{\partial L_a}{\partial t} = -\vec{\nabla}\cdot\vec{q}_\phi \qquad (5)$$

$$\text{Sedimentation}: \quad \frac{\partial z_\eta}{\partial t} = \frac{\partial}{\partial t}(h - L_a) > 0 : \mathcal{F}_\eta = \mathcal{F}$$

$$\text{Erosion}: \quad \frac{\partial z_\eta}{\partial t} = \frac{\partial}{\partial t}(h - L_a) < 0 : \mathcal{F}_\eta = \mathcal{F}_s$$

The terms on the left-hand side of (5) represent the bottom changes, changes in the sediment distribution in the active layer, and changes in the thickness of the active layer due to exchange of sediment with the substrate, respectively. Furthermore, $\vec{q}_\phi$ is the volumetric flux per unit width of grains of size ϕ, including pores. In the initial growth stage of bed forms, sorting can be seen as the rearrangement of material in the active layer with negligible interaction between substrate and active layer [*Ribberink*, 1987; *Seminara*, 1995]. This assumption, which implies that $\mathcal{F}_\eta = \mathcal{F}$, is adopted here.

[15] We consider a discrete number (N) of grain sizes, such that $\mathcal{F}(\phi) = \sum_{i=1}^{N} \mathcal{F}_i \delta(\phi - \phi_i)$, with δ the Dirac delta function. Furthermore, we use the fact that the morphodynamic timescale is much larger than the hydrodynamic timescale. This implies that the bed evolution for a discrete distribution of grain sizes and grains in class i (and diameter d_i) is given by

$$\mathcal{F}_i \frac{\partial h}{\partial t} + L_a \frac{\partial \mathcal{F}_i}{\partial t} = -\vec{\nabla}\cdot\langle\vec{q}_i\rangle \qquad (6)$$

Note that the sediment flux is averaged over the wave cycle. Together with the constraint $\sum_{i=1}^{N} \mathcal{F}_i = 1$ a closed system of equations is specified if $\vec{q}_i$ is known.

2.4. Sediment Transport

[16] *Calvete et al.* [2001b] demonstrated that both bed load and suspended load fluxes are needed to describe the growth and migration of the shoreface-connected ridges. The sediment flux, therefore, reads

$$\vec{q}_i = \vec{q}_{bi} + \vec{q}_{si}$$

where $\vec{q}_{bi}$ and $\vec{q}_{si}$ represent the bed load and suspended load contributions, respectively.

2.4.1. Bed Load

[17] The transport of sediment of class i depends on the shear stress exerted by the flow on the bed and on the grain properties. A general formulation for bed load transport of grains with size d_i over a flat bed is [*Ribberink*, 1987]: $q_{bi} \propto \mathcal{F}_i \sqrt{g' d_i^3}\,\Theta_i^{\frac{b}{2}}$. Here $g' = g(\rho_s - \rho)/\rho$, $\rho_s = 2650$ kg m^{-3} is the density of the grains, $\rho = 1030$ kg m^{-3} is the water density and b is an exponent. In the case of uniform sediment the Shields parameter $\Theta_{i,u}$ is

$$\Theta_{i,u} = \frac{\tau}{\rho g' d_i} = \frac{u_*^2}{g' d_i} \quad \text{and} \quad \Theta_{i,u} = \frac{d_m}{d_i}\Theta_m$$

In this expression τ is the bed shear stress, u_* the friction velocity, d_m the mean grain size of a mixture, and Θ_m the Shields parameter corresponding to grains of size d_m. In a sediment mixture, the effective Shields parameter Θ_i of sediment of size class i differs from $\Theta_{i,u}$. This is because the behavior of a sediment mixture is influenced by the effect of dynamic hiding: finer grains feel fluid drag less intensely than larger grains. The effect is modeled by

$$\Theta_i = \frac{1}{\xi_i}\Theta_{i,u} = \frac{1}{\xi_i}\frac{d_m}{d_i}\Theta_m \qquad (7)$$

with $\xi_i = \xi(d_i)$ a (dynamic) hiding function. According to field and laboratory data, ξ_i decreases with d_i/d_m. Thus, fine sand is less exposed to the shear stress than coarse sand. The effect of ξ_i is incorporated in a vectorial form of the bed load transport as follows:

$$\vec{q}_{bi} = \mathcal{F}_i \hat{q}\sqrt{g' d_m^3}\left(\frac{\Theta_m}{\xi_i}\right)^{\frac{3}{2}}\left[\frac{\vec{\tau}}{|\vec{\tau}|} - \lambda_b \vec{\nabla} h\right]$$

The exponent $b = 3$ is chosen consistent with the arguments presented by *Bailard* [1981] and $\hat{q}$ is a constant. Note that static hiding effects related to the presence of a critical shear stress for erosion [see *Ribberink*, 1987; *Seminara*, 1995] are not modeled. Furthermore, it is assumed that all grains are transported in the same direction: $\vec{\tau}/|\vec{\tau}|$ is independent of the grain size and the effect of bottom slopes (see the discussion by *Fredsøe and Deigaard* [1992, and references therein]) are explicitly accounted for. The bottom perturbations are given by h and λ_b is a parameter that accounts for the gravitational effect of sediment movement on a sloping bottom. For simplicity we assume λ_b to be constant ($\sim$1).

[18] The bottom shear stress vector used in the sediment transport is given by $\vec{\tau} = \rho c_f |\vec{v}_t| \vec{v}_t$. In this expression $\vec{v}_t$ is the total velocity, which consists of a wave-averaged velocity $\vec{v}$, as used in the hydrodynamic equations, and a wave contribution $\hat{u}_w$ ($\vec{v}_t = \vec{v} + \hat{u}_w$). A constant skin friction

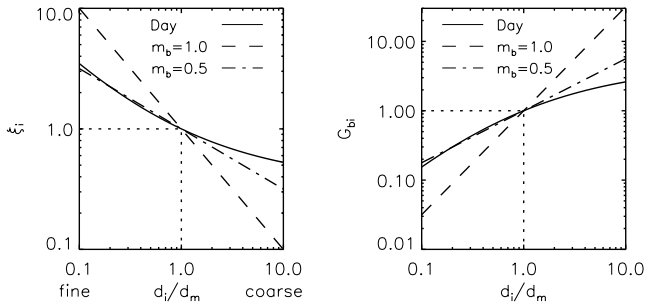

Figure 4. Different dynamic hiding functions ξ_i for the bed load sediment transport and the corresponding transport capacity functions G_{bi} as a function of d_i/d_m. Here, d_i is the grain size class i, d_m the mean grain size and $m_b \equiv \frac{2}{3}c_b$. For further information, see the text.

coefficient $c_f \sim 2 \times 10^{-3}$ is assumed. Application of these assumptions results in

$$\vec{q}_{bi} = \nu_b \mathcal{F}_i \mathcal{G}_{bi} |\vec{v}_t|^3 \left[\frac{\vec{v}_t}{|\vec{v}_t|} - \lambda_b \vec{\nabla} h \right] \qquad \mathcal{G}_{bi} = \left(\frac{1}{\xi_i} \right)^{\frac{3}{2}} \tag{8}$$

where $\nu_b = \hat{q} c_f \sqrt{c_f} / g' \sim 2 \times 10^{-5}$ s^2 m^{-1} and $\mathcal{G}_{bi}$ is the bed load transport capacity function for sediment of size d_i. A simple hiding function is used: $\xi_i = (d_m/d_i)^{m_b}$. In Figure 4, the dynamic hiding function according to Day (see in the study of *Ribberink* [1987]) and two simplified relations are shown ($m_b = 0.5$ and $m_b = 1$), together with the corresponding transport capacity functions. Note that grains of a diameter equal to d_m experience no hiding effects ($\xi_i = 1$).

[19] As was discussed in section 2.3, the model for shoreface-connected ridges requires information about the wave-averaged bed load flux, $\langle \vec{q}_{bi} \rangle$, during storms. In that case the amplitude of wave-orbital motion is much larger than the mean current, thus $u_w \gg |\vec{v}|$. Furthermore, the waves are supposed to be almost parallel to the current, leading to

$$\langle \vec{q}_{bi} \rangle = \mathcal{F}_i \mathcal{G}_{bi} \vec{q}_b \quad , \quad \vec{q}_b \simeq \frac{3}{2} \nu_b \left(u_w^2 \vec{v} - \frac{8}{9\pi} \lambda_b u_w^3 \vec{\nabla} h \right)$$

$$\mathcal{G}_{bi} = \left(\frac{d_i}{d_m} \right)^{c_b}, \qquad c_b \equiv \frac{3}{2} m_b \tag{9}$$

We use $m_b = 0.5$, which yields $c_b = 0.75$ for the exponent in the transport capacity function.

2.4.2. Suspended Load

[20] During storms it has been observed that the sediment on the inner shelf is mainly transported as suspended load [*Green et al.*, 1995]. The vectorial formulation of the suspended load flux reads

$$\vec{q}_{si} = C_i |\vec{v}_t| \left[\frac{\vec{v}_t}{|\vec{v}_t|} - \lambda_s |\vec{v}_t| \vec{\nabla} h \right] \tag{10}$$

In (10), C_i is the depth-integrated volume concentration of grains in class i, which includes all grain size dependence, and λ_s is the bed slope coefficient for suspended load transport. Since C_i is a monotonically increasing function of the bed shear stress τ, this formulation is consistent with that of *Bailard* [1981]. However, it is modified for strong forcing conditions, whereas Bailard's expression was derived for relative moderate forcing conditions. This adjustment is also motivated by the analysis preformed by *Bayram et al.* [2001], who demonstrated that Bailard's formulation underestimates the observed transport during storms. An expression for C_i is derived in Appendix A. In the case of fine sand, an approximate balance between sediment erosion and deposition near the bed exists, yielding

$$C_i = \mathcal{F}_t \delta_i E_i D \tag{11}$$

In this expression, E_i is the dimensionless entrainment of grains of diameter d_i and δ_i is the ratio of the thickness of the suspended load layer of these grains over the total water depth D, which is inversely proportional to the settling velocity w_{si} of grains in size class i.

[21] Two (out of many) formulations for the entrainment are considered, of which one is derived for sediment mixtures and one for uniform sediment. The formulation according to *Van Rijn* [1993] is $E_i \propto |\vec{v}_t|^3$ and is tested against laboratory experiments for uniform sediment. In previous work on shoreface-connected ridges this formulation was used [*Calvete et al.*, 2001b]. We use the *Garcia and Parker* [1991] formulation, which is based on results from experiments carried out with sediment mixtures, thereby accounting for possible hiding effects. The result is that $E_i \propto |\vec{v}_t|^5$ (for the complete expressions, see Appendix A). Similar to the hiding expression for bed load (7), we write

$$\delta_i E_i = \zeta_i [\delta_i E_i]_u \equiv \mathcal{G}_{si} \delta_m E_{m,u} \tag{12}$$

with ζ_i the hiding function for the entrainment of sediment and δ_m is related to the thickness of the suspended load layer for grains with size d_m. The quantity $E_{m,u}$ is the entrainment of grains of diameter d_m only. The hiding function according to *Garcia and Parker* [1991] is

$$\zeta_i = \left[\lambda_E \left(\frac{d_i}{d_m} \right)^{m_E} \right]^5 \tag{13}$$

The parameter m_E defines the importance of hiding for the entrainment of sediment, its default value is $m_E = 0.2$. A straining parameter, $\lambda_E = 1 - 0.288\sigma$, is used with σ the standard deviation on the ϕ scale, as defined in section 2.2. It models the reduced mobility of the sediment mixture as its standard deviation increases and corrects for the otherwise overestimated entrainment rates. The entrainment of grains from all size classes decreases with increasing standard deviation of the sediment mixture in the active layer. Substituting expression (13) in (12), in combination with the results from Appendix A, yields for the transport capacity function of suspended load

$$\mathcal{G}_{si} = \lambda_E^5 \left(\frac{d_i}{d_m} \right)^{c_s}, \qquad c_s \equiv 5 m_E + 4.5 - 6 e_w \tag{14}$$

The first value in the definition of c_s incorporates hiding effects, whereas the second includes the dependence of the entrainment function on the particle Reynolds number. The

coefficient e_w defines the dependence of the settling velocity on the grain size: $w_{si} \propto d_i^{e_w}$. The formulation of Hallermeier [see *Soulsby*, 1997] for fine to coarse sand yields $e_w = 1.1$, resulting in $c_s = -1.1$. Another formulation by *Van Rijn* [1993] for settling of grains in the sand range gives $e_w = 1.0$, resulting in $c_s = -0.5$. The negative value of the exponent physically means that the depth-integrated concentration for grains with sizes smaller than the mean is larger than for grains of sizes larger than the mean grain size. Combining (11)–(14) yields for the concentration

$$C_i = \mathcal{F}_i \mathcal{G}_{si} C \quad C = \delta_m E_{m,u} D = \delta_m \hat{E}_{m,u} |\vec{v}_t|^5 D$$

with $\hat{E}_{m,u}$ a constant and $\delta_m \sim 0.19$. The averaged suspended load flux (10) during storms reads

$$\langle \vec{q}_{si} \rangle = \mathcal{F}_i \mathcal{G}_{si} \vec{q}_s \tag{15}$$

with $\mathcal{G}^{si}$ defined in (14) and

$$\vec{q}_s \simeq \frac{32}{5\pi} \delta_m \hat{E}_{m,u} D \left(u_w^5 \vec{v} - \frac{1}{7} \lambda_s u_w^7 \vec{\nabla} h \right)$$

3. Basic State, Stability Analysis, and Solution Procedures

3.1. Basic States

[22] We investigate the possible onset of bed forms as free morphodynamic instabilities on a planar morphology. The basic state is uniform in the alongshore direction, with a shore-parallel current $V(x)$. The corresponding bottom profile is sketched in Figure 2. The grain size distribution function F_i for the basic state can have an arbitrary structure in the cross-shore (x) direction without violating the equilibrium conditions. In this paper, we assume that F_i is independent of this coordinate. The basic state is characterized by

$$u = 0 \qquad v = V(x) \quad z_b = -H(x) \quad z_s = \zeta(x,y)$$
$$r = r_0(x) \quad \mathcal{F}_i = F_i \quad \phi_m = \Phi_m \qquad \sigma = \sigma_0$$

From the alongshore momentum balance (1) for the basic state, it follows that

$$V(x) = \frac{\tau_{sy}/\rho - g s_0 H}{r_0}$$

The basic state velocity consists of a steady component, which is driven by a prescribed alongshore free surface pressure gradient $s_0 \equiv \partial\zeta/\partial y \sim 2 \times 10^{-7}$ and an alongshore wind stress $\tau_{sy} \sim -0.25$ N m^{-2}, such that the characteristic basic state velocity is $U = |V| \sim 0.4$ m s^{-1} at $x = 0$ in the negative y direction. This is a representative value of the storm-driven flow on the American Atlantic inner shelf [*Niedoroda and Swift*, 1981; *Lentz et al.*, 1999].

[23] The characteristic magnitude of suspended load transport $Q_s = \frac{32}{5\pi} C_0 U$ is defined for uniform sediment of a grain size d_m, with a representative value for the depth-integrated volume concentration of $C_0 = \delta_m \hat{E}_{mu} U_w^5 H_0 \sim 7.5 \times 10^{-4}$ m. For bed load transport the scale is $Q_b = \frac{3}{2} \nu_b U_w^2 U$ and the rate of bed over suspended load transport is $Q_b/Q_s \sim 0.016$.

3.2. Stability Analysis

[24] The stability of the basic state is considered by studying the evolution of small perturbations on this state. The linearized momentum and mass conservation equations are solved for a fixed bed level to find the perturbed velocity field as a function of the bottom topography. The flow variables are substituted in the bottom evolution equation to compute the changes in the bed.

3.2.1. Hydrodynamics

[25] We consider solutions of the hydrodynamic equations (1) and (2) of the following form:

$$\begin{aligned} \vec{v} &= (0, V(x)) + (u'(x,y,t), v'(x,y,t)) \\ z_s &= \zeta(x,y) + \eta'(x,y,t) \\ z_b &= -H(x) + h(x,y,t) \\ r &= r_0(x) + r'(x,y,t) \end{aligned}$$

The perturbations (indicated by primes) are assumed to be small. The expressions for r_0 and r' are given in Appendix B. The linearized versions of the momentum equation (1) are

$$V \frac{\partial u'}{\partial y} - f v' = -g \frac{\partial \eta'}{\partial x} + \frac{\tau_{sx}}{\rho} \frac{h}{H^2} - r_0 \frac{u'}{H} \tag{16}$$

$$u' \frac{\partial V}{\partial x} + V \frac{\partial v'}{\partial y} + f u' = -g \frac{\partial \eta'}{\partial y} + s_0 \frac{h}{H} + r_0 \frac{v'}{H} - r' \frac{V}{H} \tag{17}$$

and for mass conservation (2):

$$H \frac{\partial u'}{\partial x} + \frac{\partial H}{\partial x} u' + H \frac{\partial v'}{\partial y} - V \frac{\partial h}{\partial y} = 0 \tag{18}$$

3.2.2. Two-Size Mixture

[26] As with perturbations in the hydrodynamics, small perturbations in the probability distribution function $\mathcal{F}_i$ are assumed, resulting in small perturbations in the mean grain size and standard deviation:

$$\mathcal{F}_i = F_i + f_i(x,y,t) \quad \phi_m = \Phi_m + \phi_m'(x,y,t)$$
$$\sigma = \sigma_0 + \sigma'(x,y,t)$$

In this paper a two-size sand mixture is considered, with d_1 and d_2 the grain diameters of the fine and coarse size fraction, respectively ($\phi_1 \geq \phi_2$). A mean grain size of medium sand, characteristic of inner shelf sediment, is $d_m = 0.35$ mm or $\phi_m = 1.5$. The constraint on the distribution function yields:

$$F_1 + F_2 = 1 \qquad f_1 = -f_2 \tag{19}$$

The expressions for the mean grain size and the standard deviation (as defined in section 2.2) simplify to

$$\Phi_m = \phi_1 F_1 + \phi_2 F_2 \quad \sigma_0^2 = F_1 F_2 (\phi_1 - \phi_2)^2$$

From this, we derive an expression for ϕ_1 and ϕ_2 in terms of the mean grain size and the standard deviation:

$$\phi_1 = \Phi_m + \sigma_0\sqrt{\frac{F_2}{F_1}} \qquad \phi_2 = \Phi_m - \sigma_0\sqrt{\frac{F_1}{F_2}} \tag{20}$$

[27] Using the expressions given above, the perturbations in the mean grain size and standard deviation read

$$\phi'_m = \frac{\sigma_0}{\sqrt{F_2F_1}}f_1 \qquad \sigma' = \frac{\sigma_0(F_2 - F_1)}{2F_2F_1}f_1 \tag{21}$$

3.2.3. Sediment Dynamics

[28] The sediment flux consists of a bed load and a suspended load part: $\langle\vec{q}_{bi}\rangle = \mathcal{F}_i\mathcal{G}_{bi}\vec{g}_b$ and $\langle\vec{q}_{si}\rangle = \mathcal{F}_i\mathcal{G}_{si}\vec{q}_s$ (see expressions (9) and (15)). In particular,

$$\vec{q}_b = \vec{q}_{b0}(x) + \vec{q}'_b(x,y,t) \quad \mathcal{G}_{bi} = G_{bi} + g_{bi}(x,y,t)$$
$$\vec{q}_s = \vec{q}_{s0}(x) + \vec{q}'_s(x,y,t) \quad \mathcal{G}_{si} = G_{si} + g_{si}(x,y,t)$$

In the basic state only an alongshore transport component, which depends on the distance x to the shoreface, is present. Thus $\vec{\nabla}\cdot(F_iG_{bi}\vec{q}_{b0}) = \vec{\nabla}\cdot(F_iG_{si}\vec{q}_{s0}) = 0$. The transport capacity functions G_{bi}, G_{si} and the perturbations g_{bi}, g_{si} for bed load and suspended load are defined in Appendix C. Following the formulation for the roughness length k_s we use $L_a = d_m\,2^{\sigma}$ (see Appendix B); the thickness of the active layer in the basic state corresponds to $L_{a0} = 2^{\sigma_0 - \Phi_m}$. The linearized form of (6) is

$$F_i\frac{\partial h}{\partial t} + L_{a0}\frac{\partial f_i}{\partial t} = -\vec{\nabla}\cdot\langle\vec{q}'_i\rangle \tag{22}$$

where

$$\langle\vec{q}'_i\rangle = F_iG_{bi}\vec{q}'_b + \vec{q}_{b0}(G_{bi}f_i + F_ig_{bi}) + F_iG_{si}\vec{q}'_s + \vec{q}_{s0}(G_{si}f_i + F_ig_{si})$$

Summation of (22) over all size fractions, combined with the constraint on the distribution function, leads to an equation that relates the bed evolution to the sum of the sediment flux over all sizes. Back substitution of this result into (22) yields the evolution of the probability function f_i. For two-size fractions (i = 1, 2) the final equations read

$$\frac{\partial h}{\partial t} = -\left[\vec{\nabla}\cdot\langle\vec{q}'_1\rangle + \vec{\nabla}\cdot\langle\vec{q}'_2\rangle\right] \tag{23}$$

$$L_{a0}\frac{\partial f_1}{\partial t} = F_1\vec{\nabla}\cdot\langle\vec{q}'_2\rangle - F_2\vec{\nabla}\cdot\langle\vec{q}'_1\rangle \tag{24}$$

where

$$\vec{\nabla}\cdot\langle\vec{q}'_1\rangle = G_{b1}\left\{F_1\vec{\nabla}\cdot\vec{q}'_b + q_{b0}(F_1T_{b5} + 1)\frac{\partial f_1}{\partial y}\right\} + G_{s1}\left\{F_1\vec{\nabla}\cdot\vec{q}'_s + q_{s0}(F_1T_{s5} + 1)\frac{\partial f_1}{\partial y}\right\}$$

$$\vec{\nabla}\cdot\langle\vec{q}'_2\rangle = G_{b2}\left\{F_2\vec{\nabla}\cdot\vec{q}'_b + q_{b0}(F_2T_{b5} - 1)\frac{\partial f_1}{\partial y}\right\} + G_{s2}\left\{F_2\vec{\nabla}\cdot\vec{q}'_s + q_{s0}(F_2T_{s5} - 1)\frac{\partial f_1}{\partial y}\right\}$$

The quantity f_2 is eliminated by using (19) and for a two-size mixture g_{b1}, g_{s1}, g_{b2}, and g_{s2} are expressed in perturbations of the probability function f_1 (Appendix C). Also the expressions for q_{b0}, q_{s0}, $\vec{\nabla}\cdot\vec{q}'_b$ and $\vec{\nabla}\cdot\vec{q}'_s$ are given in this appendix. Equations (23), (24), and (19) give the set of equations to be solved for h and f_1. Together with (16), (17), and (18), they form a closed system.

[29] Boundary conditions are that $u' = 0$ and $h = 0$ at the transition from the shoreface to the inner shelf ($x = 0$) and for $x \to \infty$. Furthermore, periodicity in the alongshore direction is assumed.

3.3. Solution Procedure

[30] The solutions for the bottom perturbations are topographic waves, which propagate along the shelf and have a certain cross-shelf structure. They are of the form $h(x, y, t) = Re\{\hat{h}(x)e^{iky+\ \Omega t}\}$: a similar expression holds for f_1. Here k is the alongshore wave number and Ω the complex frequency. The stability analysis yields, for each wave number k, solutions for Ω; its real part Ω_r being the growth rate, with Ω_r^{-1} the e-folding timescale. Furthermore, the imaginary part Ω_{Im} is the frequency. The migration velocity of the perturbation is obtained from $c = -\Omega_{Im}/k$. For a fixed value of the alongshore wave number k the different values of Ω correspond to different cross-shore modes.

[31] Of specific interest are growing perturbations, which have $\Omega_r > 0$. The perturbation for which a maximum in the growth rate is found is called the preferred mode. The perturbed velocity u' is expressed in the bottom perturbation h, by eliminating the free surface η' from the momentum equations and using mass conservation to express v' in u'. In this study, the bottom friction is related to the grain size, thus a part of u' is related to f_1. Solving the equation for u' and substituting this in (23) and (24) results in an eigenvalue problem, which determines the cross-shore structure of h and f_1.

[32] (24) can be simplified, because the term on the left-hand side is a factor $L_{a0}/H_0 \ll 1$ smaller than the contributions on the right-hand side and can therefore excluded. This factor was derived from (23), which defines the scale for the divergence of the sediment fluxes. The result is a decoupled set of equations for the bottom and the fraction of fine grains. Consequently, the eigenvalue problem for h and f_1 is reduced to a single eigenvalue problem for h and f_1 is an algebraic function of h. Therefore, the fine grain fraction adapts instantaneously to changes in the bottom. Solutions of these equations were obtained by numerical methods.

4. Results

[33] In this section, the influence of the nonuniformity of the sediment on growth rates, migration velocities and wavelengths of the resulting bed forms is investigated. Furthermore, the resulting spatial variations in mean grain size and bottom topography are presented. Different experiments were performed, with particular emphasis on the sensitivity of the model results to the formulation of the hiding functions and the properties of the sediment. First, the influence of variation in sediment sizes was studied by varying the standard deviation of the distribution. Next, the

Table 1. Parameter Values for Uniform and Bimodal Sediment

	Uniform (Figure 5)	Bimodal (Figures 5 and 7 (t))	Bimodal (Figures 5 and 7 (b))	Bimodal (Figure 6)	Bimodal (Figure 8)
σ_0	0	0.2	1.0	0.5	0.5
F_1	1	0.5	0.5	0.5	0.7
F_2	0	0.5	0.5	0.5	0.3
Φ_m	1.5	1.5	1.5	1.5	1.5
ϕ_1	1.5	1.7	2.5	2.0	1.8
ϕ_2	1.5	1.3	0.5	1.0	0.7
d_1 (mm)	0.35	0.31	0.18	0.25	0.28
d_2 (mm)	0.35	0.41	0.71	0.50	0.60

sensitivity of the results to the hiding coefficients for bed and suspended load was investigated.

4.1. Parameter Values

[34] Values for the characteristic length and velocity scales were given in sections 2.1 and 3.1, respectively. An overview of the parameter values used for the different experiments is presented in Table 1; they are representative of conditions on Long Island inner shelf and are partly extracted from the studies of *Figueiredo et al.* [1982] and *Schwab et al.* [2000]. Note that the sediment has the same mean grain diameter in all experiments, while the diameters of the fine and coarse grains were allowed to vary.

4.2. Standard Deviation

[35] The influence of the standard deviation of the mixture on the characteristics of the ridges was investigated. For a fixed mean grain size, the standard deviation of the sediment was varied over a range, such that d_1 and d_2 are in the fine to coarse sand range. In this section, the default values of $c_b = 0.75$ and $c_s = -1.1$ are used. Figure 5 shows the changes in the growth rate and migration velocity of the most unstable mode (first cross-shore mode) for each wave number and for different values of the standard deviation. Values are scaled by those of the preferred mode in the case of uniform sediment ($\sigma_0 = 0$). The maximum growth rate for uniform sediment is $\Omega_{ru} = 8.6 \times 10^{-3}$ yr^{-1}, attained for wave number $k_u = 1.9$ km^{-1} and the corresponding migration speed is $c_u = -0.9$ m yr^{-1}. The alongshore spacing between successive crests is $\lambda^* = 2\pi k_u^{-1} = 3.2$ km, and the timescale for the growth is $\Omega_{ru}{}^{-1} = 117$ yr. In the computations of the timescale it was assumed that storms prevail during a time fraction $\mu = 0.05$, whereas no growth of perturbations occurs during the remaining time fraction. Here we use the formulation for the entrainment of suspended sediment by *Garcia and Parker* [1991]. In the case of $\sigma_0 = 0$, the growth rate and migration curves are similar to those obtained with the *Van Rijn* [1993] formulation, as was used by *Calvete et al.* [2001b].

[36] A clear stabilizing effect on growth rates of the bimodal mixture, as compared to uniform sediment, is found if the standard deviation is increased (Figure 5). This goes along with a (small) decrease of the wave number, i.e., increase in wavelength, of the bed forms. The migration velocities are enhanced. The maximum growth rate is reduced by ~50% for a bimodal sediment mixture with a standard deviation of $\sigma_0 = 0.5$. Migration velocities for this case increase to -1.2 m yr^{-1}. The fastest growing perturbation in this case has a wavelength $\lambda^* = 3.4$ km, and its spatial pattern is shown in Figure 6. The elevation of the bottom is indicated by the dark and light colors. The contour lines are those of the fraction of fine grains (with diameter d_1). More fine sediment ($f_1 > 0$) results in an increase in the mean grain size in phi units ($\phi'_m \propto f_1$). The results indicate that f_1 is positive on the downcurrent (seaward) flank of the ridges, hence the mean grain size becomes finer in this area and coarser on the upcurrent (landward) flank. The perturbed bottom topography and the perturbed mean grain size patterns are approximately 90° out of phase. Note that the basic state velocity is directed from the top to the bottom of this figure ($V < 0$), so that the ridges are characterized by an upcurrent rotation.

[37] The locations of the maxima and minima in the mean grain size depend on the value of the standard deviation σ_0 (or sorting index). Figure 7 shows a shore-normal cross section of the bottom topography and fraction of fine grains for two different sorting indices. A decrease in the phase difference between the two patterns is found for larger values of the standard deviation. An interpretation of these results will be given in section 5.

[38] Experiments were conducted to investigate the sensitivity of the model results to different values of the parameter F_1. It was found that, if the fraction of fine grains $F_1 > 0.5$, the influence of the standard deviation on the bed form characteristics (wavelength, growth rate and migration speed) becomes stronger. On the contrary, if $F_1 < 0.5$ (more coarse grains than fine grains), these dependencies become weaker. Changing the value of F_1 does not affect the bottom pattern or the distribution of the mean grain size of Figure 6, but a different sorting pattern is obtained. In the case of $F_1 = 0.5$ it follows that $\sigma' = 0$ according to (21), hence no

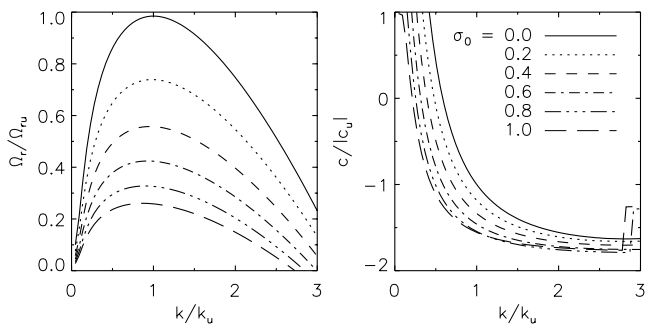

Figure 5. Growth rates (left) and migration velocities (right) of the first cross-shore mode as a function of the wave number k (scaled by the preferred mode for uniform sediment) for different values of σ_0. The parameters used for the bimodal mixtures are $F_1 = 0.5$, $c_b = 0.75$, and $c_s = -1.1$.

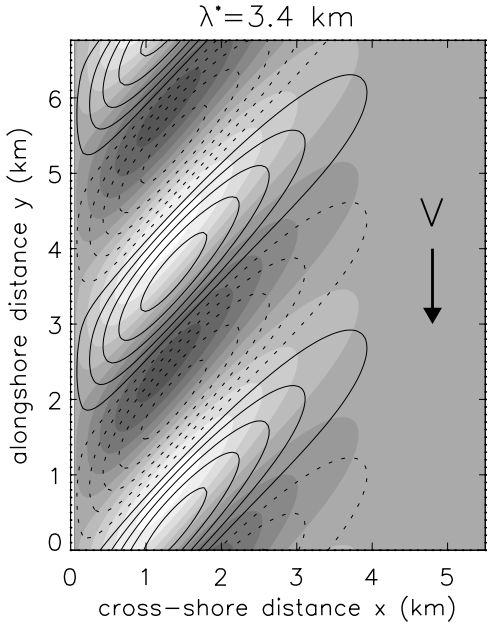

Figure 6. Bottom perturbations (colors; light: bars, dark: troughs) and perturbations in the fraction of fine grains (lines; solid: $f_1 > 0$, dotted: $f_1 < 0$) for $\sigma_0 = .0.5$, $F_1 = 0.5$, $c_b = 0.75$, and $c_s = -1.1$. The arrow indicates the direction of the basic state velocity.

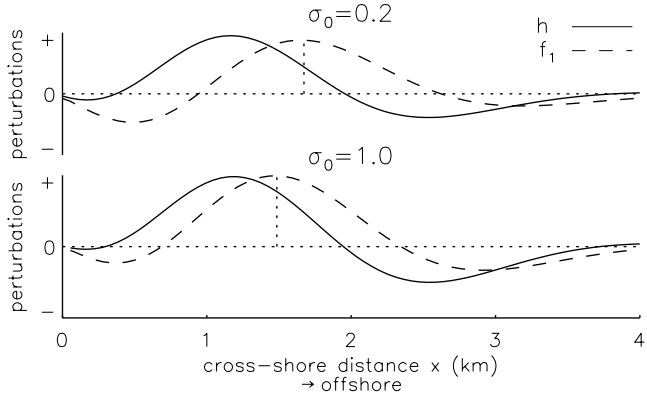

Figure 7. Cross sections through a ridge, normal to shore, of perturbations in bottom, h, and in the fraction of fine grains, f_1 (or similar in mean grain size, ϕ'_m). Quantities are scaled by their maximum values and shown for $F_1 = 0.5$ and a small standard deviation of the mixture (top: $\sigma_0 = 0.2$) as well as for a large value (bottom: $\sigma_0 = 1.0$). Furthermore, $c_b = 0.75$ and $c_s = -1.1$.

changes in the standard deviation occurred. In Figure 8, it is shown that for $F_1 = 0.7$ the sediment located on the seaward flank is finer ($\phi'_m > 0$) and better sorted ($\sigma' < 0$) than sediment on the landward flank, which is coarser and more poorly sorted ($\sigma' > 0$).

4.3. Hiding Functions: Bed Load

[39] The characteristics of both the preferred bottom mode and the grain size distribution also depend on the coefficient c_b in the hiding function of the bed load transport, defined in (9). Therefore, experiments were conducted in which c_b was varied. Physically this means that the hiding effects in the bed load transport were reduced or enhanced. The coefficient for the hiding in suspended load was kept constant at its default value $c_s = -1.1$.

[40] In Figure 9, the characteristics of the preferred mode are shown as a function of the standard deviation for different values of c_b. The maximum growth rate Ω_{rmax}, migration velocity c_{max} and preferred wave number k_{max} in the bimodal sediment case are scaled by their corresponding values for uniform sediment (being k_u, Ω_{ru} and $|c_u|$). The curves show, for all cases, a reduction in the wave number and growth rates, and an enhancement in migration rate if σ_0 is increased. A value of $c_b = 0$ implies that there is no hiding, $c_b = 1.5$ corresponds to a value of $m_b = 1$ in the hiding function (see Figure 4). The new information deducted from this figure is that the inclusion of a hiding function in the bed load transport formulation has little effect on the growth of the shoreface-connected ridges, but increasing hiding effects cause larger migration speeds. An interpretation of the results will be given in section 5.

[41] In Figure 10, cross sections show the change in the distribution of the fraction of fine sediment for no hiding and strong hiding in the bed load flux. In the former case the selective suspended load transport results in an almost 90° out-of-phase relation between topography and mean grain size. An increase in the strength of the hiding in bed load ($c_b > 0$) reduces this phase shift (see Figure 10, bottom).

4.4. Hiding Functions: Suspended Load

[42] The same experiments were done to investigate the dependence of model results on the hiding coefficient c_s and the straining coefficient λ_E in the transport capacity function of suspended load transport (defined in (14)). Only one of these parameters, c_s, can result in differences between the depth-integrated concentrations of the size classes in a sediment mixture, thereby introducing a mechanism for selective transport of suspended load.

[43] The value of exponent c_s is mainly determined by two factors. The first is the dependence of the entrainment and the relative thickness of the suspended load layer on the grain size (including settling velocity and particle Reynolds

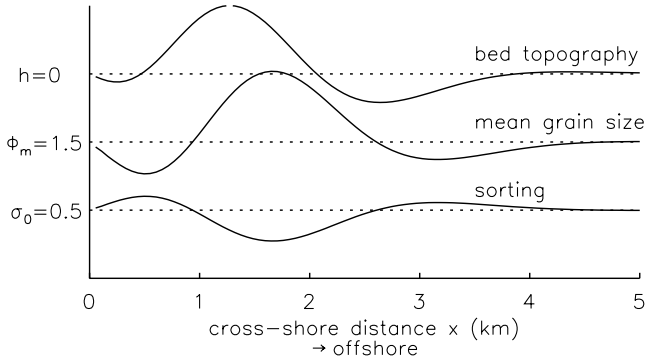

Figure 8. Cross sections through a ridge, normal to shore, of bed topography h, perturbations ϕ'_m in the mean grain size and perturbed sorting values (standard deviation) σ'. Results are shown for $F_1 = 0.7$, $\sigma_0 = 0.5$, $c_b = 0.75$, and $c_s = -1.1$.

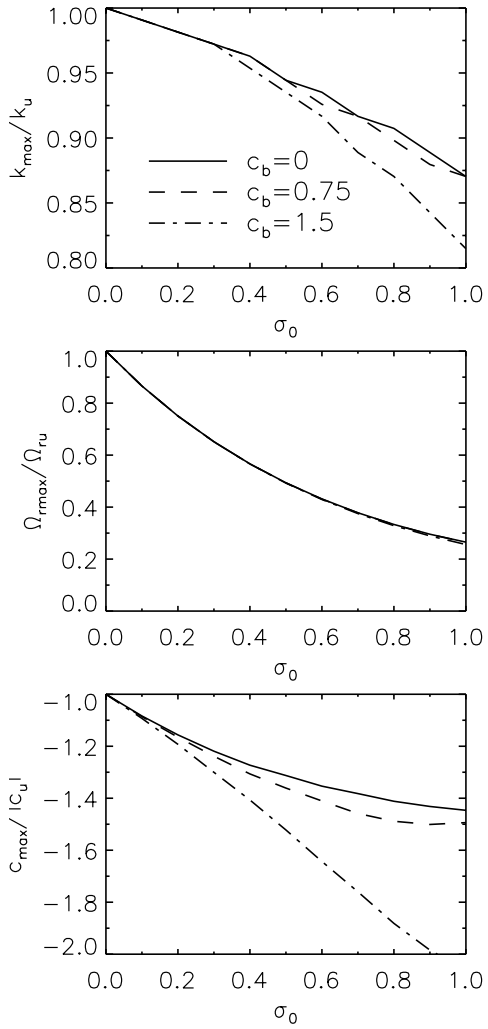

Figure 9. Wave number k_{max} of the preferred mode (scaled by its value k_u for uniform sediment), growth rates, and corresponding migration velocities as a function of the standard deviation of the mixture σ_0. Results are shown for different formulations of the hiding function in the transport of bed load, with $c_s = -1.1$ and $F_1 = 0.5$.

number). The second factor is the strength of the hiding for the entrainment of sediment in suspension, indicated by the coefficient m_E in the hiding function ζ_i(13). We only investigated the influence of the second contribution and assumed $e_w = 1.1$ (section 2.4.2), i.e., $c_s = 5m_E - 2.1$. Without hiding effects in the entrainment ($m_E = 0$), the depth-integrated concentration of fine sediment is larger than that of coarse material. The inclusion of hiding effects (default: $m_E = 0.2$) reduces the entrainment of fine sediment from the bed, nevertheless, it still results in a depth-integrated concentration of fine material that is larger than that of coarse material. In the special case of $m_E = 0.42$ it follows that $c_s = 0$, hence, $\mathcal{G}_{si}$ is independent of the grain size. The higher concentration of fine sediment, as a consequence of, for example, their smaller settling velocities, is counterbalanced by a reduced entrainment flux of fine grains from the bed due to hiding effects. These three situations are shown in Figure 11 as $c_s = -2.1$, -1.1 and 0, including the straining factor and a constant value of $c_b = 0.75$. With higher standard deviations, a decrease in wave number and growth rates and an increase in migration rates is found. The growth rates are most strongly influenced.

[44] The straining parameter λ_E in (14) reduces the suspended load flux of both size classes in the sediment mixture, whereas the reduction becomes more important for larger values of σ_0. To demonstrate the importance of this parameter, results are shown without straining ($\lambda_E = 1$) and no hiding in the entrainment ($c_s = -2.1$). Figure 11 indeed reveals a change in the results: instead of a decrease in the maximum growth rate, an increase with σ_0 is found and the migration speed is decreased. This will be discussed in more detail in section 5.

[45] The bed form and the mean grain size patterns are in phase if no grain size dependence is used in the suspended load transport ($c_s = 0$), with the finer sediment on the crests for $c_b > 0$ (see Figure 12, top). A phase shift between the mean grain size and the bed topography pattern is induced by the suspended load flux. In fact, the sediment is finer on the seaward (downcurrent) flank of the ridges for $c_s < 0$. These phase shifts do not change if the straining parameter is excluded.

5. Physical Interpretation

[46] The results presented in the previous section can be explained in physical terms. The concepts discussed here are based on mechanisms for the formation of shoreface-connected ridges under the assumption of uniform sediment, as presented earlier by *Trowbridge* [1995] and by *Calvete et al.* [2001b]. They have demonstrated that the transverse slope of the bottom plays an essential role in the formation of the ridges. An offshore deflection of the current, i.e., $u' > 0$, results in a convergence of the sediment flux and the growth of upcurrent oriented ridges. This behavior is due to mass conservation of both water and sediment. The presence of a ridge causes an enhanced convergence in both the water and sediment flux (with respect to that induced by the offshore movement of water and sand) on the downstream side of the ridge. Likewise, the convergence reduces on the upstream flank of the ridge. The result is that sediment is eroded (deposited) on the upstream (downstream) flank of the ridges. Therefore,

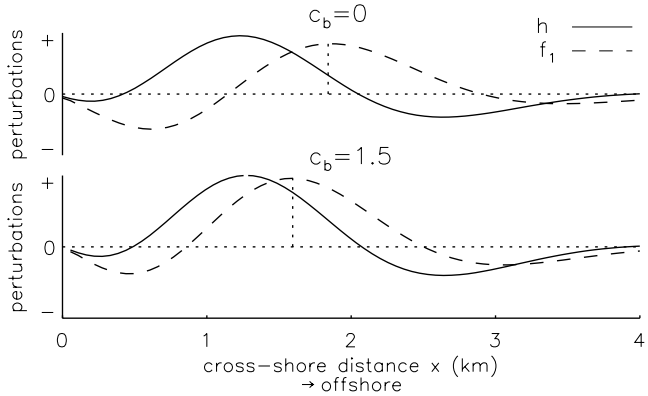

Figure 10. As in Figure 7, but for $\sigma_0 = 0.5$, $F_1 = 0.5$, $c_s = -1.1$ and $c_b = 0$ (top), $c_b = 1.5$ (bottom).

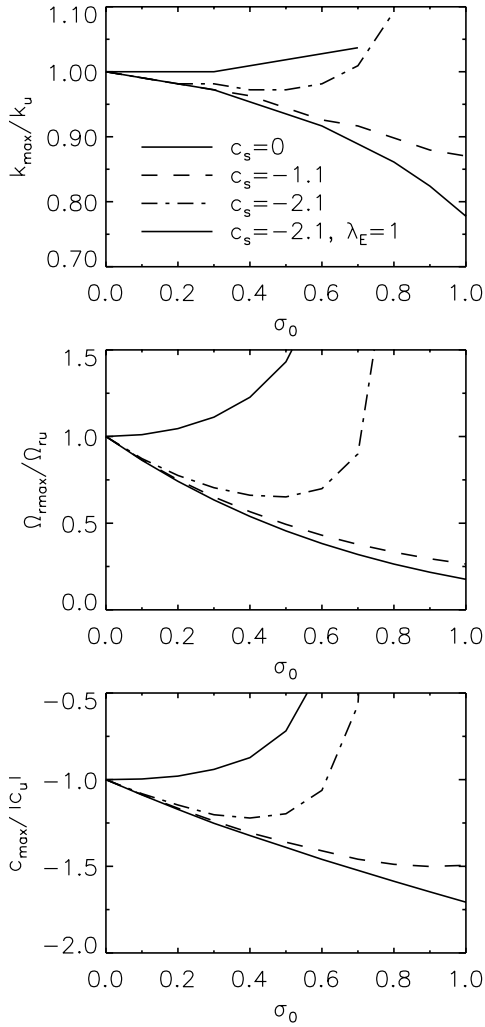

Figure 11. As in Figure 9, but now for different formulations for the hiding coefficient c_s in the suspended load transport and $c_b = 0.75$.

downcurrent migration of the ridges takes place. It appears that the growth of the shoreface-connected ridges is mainly determined by the suspended sediment flux, while bed load transport determines the downcurrent migration of the bed forms.

[47] In the case of a bimodal sediment mixture growth rates become smaller, migration rates speed up, the preferred length scale becomes longer, and sorting of sediment is observed. To understand these new features, we examined the effects of dynamic hiding in both bed load and suspended load in the bottom evolution equations (23) and (24).

5.1. Hiding in Bed Load

[48] For the exponents in the transport capacity functions for bed load and suspended load we consider: $c_b > 0$ and $c_s = 0$, respectively. These assumptions allowed for an interpretation of the results shown in Figures 11 and 12 ($c_s = 0$). The transport of suspended load is independent of the grain size, therefore only the effect of the straining parameter for suspended load and hiding in bed load are included. As a result, the equations for the evolution of the bottom and the fraction of fine sediment reduce to:

$$\frac{\partial h}{\partial t} = -T_{b2}\vec{\nabla}\cdot\vec{q}'_b - \Lambda_E^5\vec{\nabla}\cdot\vec{q}'_s - [T_{b1} + T_{b2}T_{b5}]q_{b0}\frac{\partial f_1}{\partial y} \qquad (25)$$

$$0 = -T_{b3}\vec{\nabla}\cdot\vec{q}'_b - \Lambda_E^5 q_{s0}\frac{\partial f_1}{\partial y} \qquad (26)$$

where

$$T_{b1} = G_{b1} - G_{b2} \qquad T_{b2} = F_1G_{b1} + F_2G_{b2}$$
$$T_{b3} = F_1F_2(G_{b1} - G_{b2}) \qquad T_{b4} = F_2G_{b1} + F_1G_{b2}$$

The expressions for T_{b5} and Λ_E are given in Appendix C. The left-hand side of (26) has been set to zero, following the arguments presented in section 3.3. Furthermore, since $|q_{s0}| \gg |q_{b0}|$ (suspended load dominates over bed load transport), the terms proportional to q_{b0} are omitted in (26).

[49] To understand the alongshore variation in the mean grain size we consider the expression for $\vec{\nabla}\cdot\vec{q}'_b$, as given in Appendix C, and neglect slope effects. After substitution of expression (4) for the wave-orbital velocity

$$\vec{\nabla}\cdot\vec{q}'_b \propto u_w^2\left[\left(-\frac{m}{H^{m/2}} - 1\right)\frac{1}{H}\frac{\partial H}{\partial x}u' + \frac{V}{H}\frac{\partial h}{\partial y}\right]$$

This expression is simplified by applying scaling arguments. For the parameter values, $V \sim -0.4$ m s^{-1}, $H \sim 14$ m, $\partial H/\partial x \sim 1 \times 10^{-3}$ and $m \sim 1.6$, the first term is a factor 100 smaller than the second term and is neglected. Since $q_{s0} \propto u_w^5 HV$ (Appendix C), this yields for (26):

$$\frac{\partial f_1}{\partial y} \propto -(G_{b1} - G_{b2})\frac{\partial h}{\partial y}$$

This result shows that the fraction of fine sand is either in phase or 180° out of phase with the topography. For bed load the transport capacity function is given by $G_{bi} = (d_i/d_m)^{c_b}$. If $c_b > 0$ it follows that $G_{b1} < 1 < G_{b2}$, leading to a reduced transport of fine sediment relative to the transport of coarse sediment. The relation between the

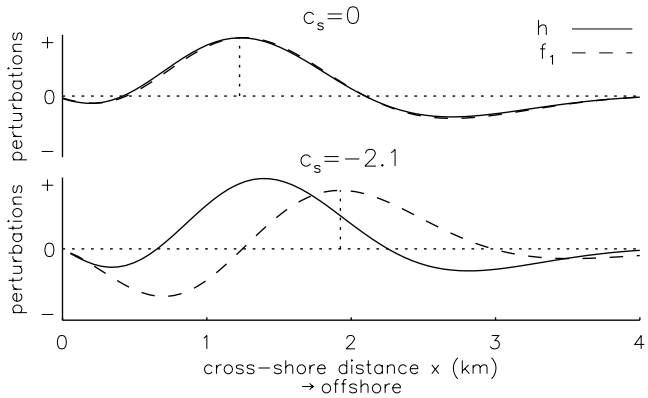

Figure 12. As in Figure 7, but for $\sigma_0 = 0.5$, $F_1 = 0.5$, $c_b = 0.75$ and $c_s = 0$ (top), $c_s = -2.1$ (bottom).

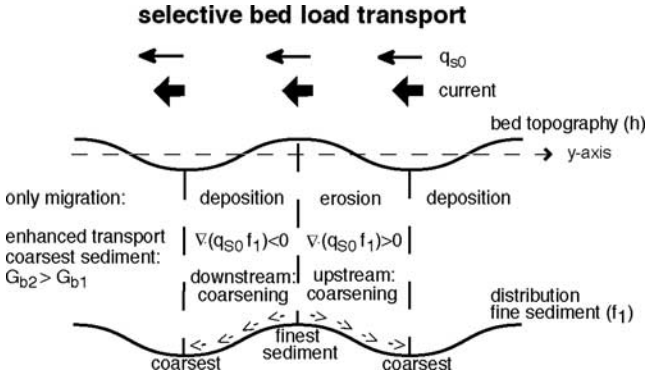

Figure 13. Schematic view of the selective bed load transport mechanism. The downcurrent migration induced by the bed load flux results in an erosion/deposition pattern, which is shifted with respect to the bed topography. Equation (26) requires the convergence rate of the bed load flux to be proportional to a changes in the alongshore (i.e., downstream) fining of the sediment. In a deposition area ($\vec{\nabla} \cdot \vec{q}'_b < 0$), therefore $q_{s0}\, \partial f_1/\partial y < 0$ for the situation where transport of coarse material is favored with respect to that of fine grains. When moving from the crest to the adjacent troughs, a coarsening of the sediment is found.

bottom topography and the fraction of fine grains is therefore given by $f_1 \propto h$ for this situation. A schematic view of this selective transport mechanism is shown in Figure 13. The mean grain size is finest on the crests of the ridges, and explains the pattern shown in Figure 12 ($c_s = 0$).

[50] The enhanced migration rates and reduced growth rates for a sediment bed composed of a bimodal mixture (Figure 11, $c_s = 0$) are understood from (25). The suspended load flux is only modified by the straining factor, when compared to uniform sediment. This factor is smaller than unity and determines the reduction of the growth rates by $\Lambda_E^5 \sim 0.2$ for $\sigma_0 = 1$ (Figure 11, middle). The bed load flux is a factor T_{b2} different from the uniform sediment case. As $T_{b2} \geq 1$ for bed load transport, hiding effects cause a faster migration compared to uniform sediment, while it hardly changes the growth. The last term (redistribution of sediment) in (25) could also change the migration, because f_1 is related to h. However, experiments indicated that this contribution is only of minor importance to the downcurrent migration.

5.2. Hiding in Suspended Load

[51] For the investigation of hiding (and straining) in suspended load we set $c_b = 0$ and $c_s < 0$. This enables an interpretation of the results shown in Figures 9 and 10 ($c_b = 0$). The equations for the evolution of the bottom and the fraction of fine sediment reduce to

$$\frac{\partial h}{\partial t} = -\vec{\nabla} \cdot \vec{q}'_b - T_{s2} \vec{\nabla} \cdot \vec{q}'_s - [T_{s1} + T_{s2} T_{s5}] q_{s0} \frac{\partial f_1}{\partial y} \qquad (27)$$

$$0 = -T_{s3} \vec{\nabla} \cdot \vec{q}'_s - [T_{s4} + T_{s3} T_{s5}] q_{s0} \frac{\partial f_1}{\partial y} \qquad (28)$$

where

$$T_{s1} = G_{s1} - G_{s2} \qquad T_{s2} = F_1 G_{s1} + F_2 G_{s2}$$
$$T_{s3} = F_1 F_2 (G_{s1} - G_{s2}) \qquad T_{s4} = F_2 G_{s1} + F_1 G_{s2}$$

Equation (28) relates alongshore changes in the fining of the bottom material to the convergence of the suspended load flux, and bed load contributions are neglected. In the second term on the right-hand side, $[T_{s4} + T_{s5} T_{s3}]$ is positive for realistic values of the parameters. In Figure 14, the mechanism for selective suspended load transport is sketched.

[52] Substitution of the expression for $\vec{q}'_s$ (Appendix C) in (28) yields

$$-V \frac{\partial f_1}{\partial y} \propto (G_{s1} - G_{s2}) \frac{\partial u_w}{\partial x} u'$$

In this expression $\partial u_w/\partial x < 0$ (waves induce less stirring of sediment in larger depth) and $V < 0$. The momentum equations are used to relate u' to h. *Calvete et al.* [2001b] showed that the perturbations in the cross-shore velocity are in phase with the bottom perturbations ($u' > 0$ if $h > 0$). Hence, if the transport in suspension is more pronounced for the finer grains ($G_{s1} > G_{s2}$), this leads to $\partial f_1/\partial y \propto -u' \propto -h$. Consequently, the pattern of the mean grain size for suspended load is approximately 90° out of phase with the topography, such that the finer sediment is found on the downcurrent flank of the ridges. This effect is clearly seen in Figure 10 (top) for $c_b = 0$ and $c_s = -1.1$.

[53] The reduced growth rates for graded sediment compared to uniform sediment can be understood from (27). Growth is mainly determined by the second term on the right-hand side, where the part related to the grain size is a factor T_{s2} different from that found in the case of uniform sediment. For selective suspended load transport, with hiding coefficient $c_s = -1.1$, the factor $T_{s2} < 1$. The presence of a straining parameter in the transport capacity function for suspended load (14) causes the total transport of the two grain sizes in a mixture to be less than the transport of sediment of a uniform grain size. A stabilizing effect is found with an increasing standard deviation of the mixture (see Figure 9, $c_b = 0$), whereas the contribution of c_s to the transport capacity function has the opposite effect. Thus, a stronger hiding in suspended load (larger values of c_s) counteracts the stabilizing effect of the straining. This explains why growth rates increase with increasing values of $|c_s|$ for a fixed value of σ_0 (see Figure 11).

[54] The bed load contribution to the migration (downcurrent) is the same as for uniform sediment, but the contribution of suspended load (upcurrent migration) decreases with increasing values of σ_0, resulting in a net enhancement of the migration in the downstream direction. An additional contribution to the bottom evolution is given by the last term in (27), which turns out to be very small.

[55] If selective transport in both suspended and bed load is included, the pattern of the mean grain size resembles that found in the case of only hiding in suspended load. This is because the suspended load flux dominates over the bed load flux. The hiding function of the bed load flux slightly modifies the 90° phase difference (induced by suspended load) between the mean grain size and bed topography. This tendency is visible in Figure 10.

[56] The standard deviation σ_0 of the mixture also influences the phase difference between the mean grain size and bottom topography. Because of the straining parameter λ_E in the selective suspended load flux, the latter decreases

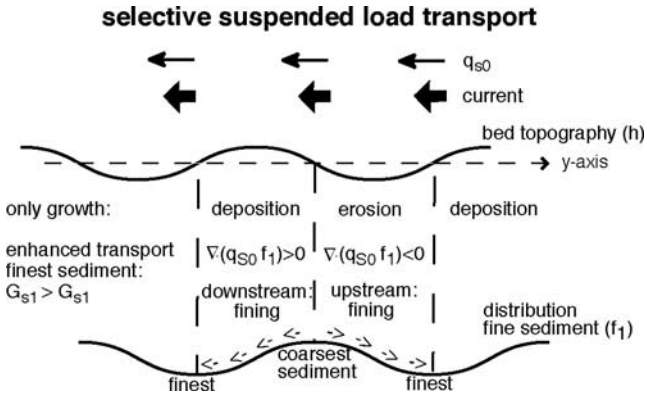

Figure 14. Schematic view of the selective suspended load transport mechanism. Suspended load mainly causes the growth of the ridges (erosion/deposition pattern almost in phase with the bottom topography). The deposition of suspended sediment is related to the gradient in the distribution of fine grains (28). In a deposition area ($\vec{\nabla} \cdot \vec{q}'_s < 0$), therefore $q_{s0}\partial f_1/\partial y > 0$ for a situation where transport of fine material is favored with respect to that of coarse sand. The result is a downstream fining in the deposition area; the finest material is located approximately $\frac{1}{4}$ wavelength downstream of the crest.

with increasing σ_0. The bed load flux is not changed by the straining parameter. This implies that the relative importance of the suspended load transport, with respect to bed load transport, decreases with increasing σ_0. Hence, the phase shift becomes smaller with increasing standard deviations, which explains the results shown in Figure 7.

6. Discussion

[57] The model results are consistent with the field data, as discussed in section 1. The data reveal the mean grain size pattern is approximately 90° out of phase with topography, with the coarsest sand on the landward flank (upcurrent), and the finest sand on the seaward (downcurrent) flank. An exception to this very consistent pattern in the mean grain size, as observed on different shelves, concerns the shoreface-connected ridges along the central Dutch coast (southern North Sea) [*Van de Meene et al.*, 1996]. No marked spatial variation in the mean grain size across the ridge topography is found, except for a weak tendency toward a better sorting (smaller standard deviations) at the crests of the ridges. A potentially important difference between the American Atlantic shelf and the Dutch shelf is the strength of the tidal current. Model experiments with both bimodal mixtures and uniform sediment showed that adding tidal currents does not change the results as presented here. This suggests that tidal currents are not the cause of the difference in the observed patterns for the Dutch coast (strong tides) and North America (weak tides).

[58] Besides the mean grain size, another aspect of the model results to be compared with the field data is the variation in the standard deviation over the ridges. For the American shelf, the most pronounced differences in sorting characteristics are seen between sediment in the crest and trough. In general, the values of standard deviation of the sediment are higher in the troughs than on the crests of the ridges [*Swift et al.*, 1972, 1978; *Schwab et al.*, 2000]. This is consistent with the sorting pattern found over the ridges along the central Dutch coast, in contrast to the lack of a variation in the mean grain size pattern. Data gathered from the German Bight [*Antia*, 1993] show that the surficial sediment found on the seaward flank are best sorted (small σ) and poorest in the troughs and on the landward flank. In the model, the variation in the sorting index is determined by relation (21). Clearly, variations in sorting across the ridges in a two-size mixture are only present in the model if the fractions of fine and coarse grains are not equal. Choosing $F_1 > F_2$ (weight percentage of fine sediment is larger than of coarse sediment) yields that in areas where positive perturbations in the mean grain size are present the material is better sorted. Combined with the effect of hiding in suspended and bed load (finer seaward flank), this case provides a good representation of the data.

[59] The results should be interpreted with care: the formulation for the selective transport of suspended and bed load are based on expressions which are found as a best fit with many different data sets [*Zyserman and Fredsøe*, 1994; *Admiraal et al.*, 2000]. These data are mostly based on measurements in shallow rivers and flume experiments and we assumed them to be also applicable to shallow coastal seas. However, in the sensitivity experiments it was shown that the general trend is the same for a large range of values of the sediment parameters, such as for the exponents in the hiding functions and the composition of the sediment mixture.

7. Conclusions

[60] In this paper a model was developed and analyzed to study the initial formation of shoreface-connected ridges and the corresponding grain size distribution on storm-dominated shelves. The model consists of the shallow water equations, a sediment transport formulation and a mass balance of sediment. The sediment is represented by two grain size classes. Both bed load and suspended load sediment fluxes are considered, as are dynamic hiding effects. The basic state represents a storm-driven flow on an inner shelf with a transversely sloping bottom. The results of the model presented here indicate that, in the case of a sediment mixture, there is a positive feedback between storm-driven currents and the eroding bottom. This confirms and generalizes earlier findings by *Trowbridge* [1995] and *Calvete et al.* [2001b] for a single grain size fraction.

[61] The first objective of this research was to investigate the influence of sediment sorting on the temporal and spatial characteristics of shoreface-connected ridges. The stabilizing effect of sediment sorting on the growth of bed forms, as found earlier in many laboratory experiments and other model studies, is also observed within the present model. Based on the experiments that were carried out, we conclude that the behavior of growth rates is determined by the formulation for the hiding in suspended load. A stabilized growth turns out to be mainly because of the presence of a straining parameter in the hiding function of suspended load. This accounts for the reduced mobility of grains in suspension with increasing standard deviations of the sediment mixture. If the straining parameter is excluded in the suspended load formulation, a destabilizing effect with

respect to uniform sediment is found. The migration of the shoreface-connected ridges is in the downcurrent direction and enhanced by the bimodal character of the sediment. Despite a suspended load flux, which is much larger than the bed load flux, the migration is controlled by the bed load flux and its hiding coefficient c_b. Wavelengths of the bed forms are only slightly affected. A spatial phase shift of approximately 90° is found between the topography and mean grain size for shoreface-connected ridges: the coarsest material occurs on the landward (upcurrent) flank. Selective transport of sediment in suspension causes this phase shift.

[62] The second objective of this study was to gain knowledge into the physical mechanism responsible for the observed grain size distribution over shoreface-connected ridges. Combining the observations with the model results, and the subsequent analysis of the equations, leads to several conclusions with respect to the physical mechanisms which could be responsible for the observed sedimentary patterns. First of all, the persistent finer downcurrent flank of the ridges and the coarser sediment on the upcurrent flank appears to be in reasonable agreement with observed grain size distributions over shoreface-connected ridges. The model results support the assumption that the transport of sediment as suspended load cannot be neglected and that the corresponding flux of fine material is larger than of coarse material. The relative importance of the bed load flux can shift the pattern of the mean grain size more in phase or out of phase with the topography. The model reproduces observed sorting patterns over the ridges (well/poorly sorted sediment on the seaward/landward side of the ridges) if the weight percentage of fine grains is larger than that of coarse grains. Another quantity that influences the phase shift is the standard deviation of the sediment: if it increases it causes a reduction in the importance of suspended load over bed load. Finally, the model results indicate that tidal currents and a grain size dependent formulation for the bottom friction coefficient do not change the sediment patterns for shoreface-connected ridges.

Appendix A: Suspended Load Concentration

[63] The suspended load flux requires knowledge of the depth-integrated volumetric concentration of sediment. The latter is governed by

$$\frac{\partial C_i}{\partial t} + \vec{\nabla} \cdot (\vec{v}_t C_i) = w_{si}(\mathcal{F}_i E_i - c_{bi}) \tag{A1}$$

The first term on the right-hand side is the flux of sediment into suspension, the second term is the deposition flux. Here w_{si} is the settling velocity of grains of size d_i, E_i is the dimensionless entrainment of these grains, and c_{bi} is the actual volume concentration near the bed. The entrainment of a size fraction is multiplied by the probability $\mathcal{F}_i$ that sediment of this grain size actually occurs.

[64] For sand mixtures on inner shelves the settling period is much smaller than the hydrodynamic timescale. This implies that (A1) reduces to an approximate balance between erosion and deposition flux near the bed:

$$\mathcal{F}_i E_i - \frac{C_i}{\delta_i D} = 0$$

The second term represents the deposition flux of these grains and is expressed in terms of the depth-integrated concentration C_i. Parameter δ_i is the ratio of the thickness of the suspended load layer of grains in class i over the total water depth D.

[65] In the study of *Garcia and Parker* [1991] an expression for the entrainment of a mixture of particles is obtained by analyzing laboratory and field data. They find

$$E_i = A(\lambda_E Z_i)^5 \quad Z_i = \frac{u*}{w_{si}} R_{pi}^{0.6} \left(\frac{d_i}{d_m}\right)^{0.2}$$

with $A = 1.3 \times 10^{-7}$ a constant. Hiding effects are covered by the last factor in the expression for Z_i. Furthermore, $\lambda_E = 1 - 0.288\sigma$ is a straining parameter, $R_{pi} = \sqrt{g' d_i^3}/\nu$ is the particle Reynolds number of grains of size d_i and $\nu = 1.36 \times 10^{-6}$ m^2 s^{-1} is the kinematic viscosity coefficient of water. The entrainment for uniform sediment (grain size d_m) reads

$$E_{m,u} = A Z_m^5 = \hat{E}_{m,u} |\vec{v}_t|^5 \quad \hat{E}_{m,u} = A \left(\frac{\sqrt{c_f}}{w_{sm}} R_{pm}^{0.6}\right)^5$$

such that Z_m corresponds the value of Z_i for $d_i = d_m$. From this result it follows that the expression for $\mathcal{G}_{si}$ in (12) is written as:

$$\mathcal{G}_{si} \equiv \zeta_i \left(\frac{\delta_i}{\delta_m}\frac{E_i}{E_m}\right)_u = \zeta_i \frac{w_{sm}}{w_{si}} \left(\frac{R_{pi}}{R_{pm}}\right)^3 \left(\frac{w_{sm}}{w_{si}}\right)^5$$

Appendix B: Bottom Friction Coefficient

[66] The expression for the grain roughness length used in the formulation for the bottom friction coefficient (see (3)) reads $k_s = 3 \cdot d_m \sigma_m$, with σ_m the geometric standard deviation, defined as $\sigma_m = 2^\sigma$. When expressed in terms of phi (section 2.2) it follows that $k_s = 3 \cdot 2^{\sigma - \phi_m}$ (defined in units of mm). Including small perturbations in the mean grain size and standard deviation in the friction parameter gives for the quantities that correspond to the basic state and the perturbation of the bottom friction parameter:

$$r_0 = \frac{2}{\pi}\frac{g\, u_w}{C_{h0}^2} \quad r' \simeq \frac{2\, r_0}{C_{h0}} \left\{ \left(\sigma' - \phi_m'\right) \ln 2 + \frac{h}{H} \right\} \tag{B1}$$

The expression for the Chezy coefficient, as defined in section 2.1 with $D = H - h$, for the basic state is $C_{h0} = C_h(H, \Phi_m, \sigma_0)$. The perturbations in the bottom friction coefficient used in the momentum equations, with r' as defined in (B1), is written in terms of the unknowns h and f_1 by using (21).

Appendix C: Sediment Flux

[67] The transport capacity functions, defined in (8) and (14) for bed load and suspended load, was split into contributions which correspond to the basic state and the perturbed state, respectively. These results are used in section 3.2.3 and read

$$\mathcal{G}_{bi} = 2^{c_b(\phi_m - \phi_i)} \qquad G_{bi} = 2^{c_b(\Phi_m - \phi_i)}$$
$$g_{bi} = c_b \ln 2\; G_{bi} \phi_m' = G_{bi} T_{b5} f_1$$

$$\mathcal{G}_{si} = \lambda_E^5 2^{c_s(\phi_m - \phi_i)} \qquad G_{si} = \Lambda_E^5 2^{c_s(\Phi_m - \phi_i)}$$
$$g_{si} = G_{si}\left[c_s \ln 2\; \phi_m' + 5\frac{\lambda_E'}{\Lambda_E}\right]$$
$$= G_{si} T_{s5} f_1$$

$$\lambda_E = 1 - 0.288\sigma \qquad \Lambda_E = 1 - 0.288\sigma_0$$
$$\lambda_E' = -0.288\sigma'$$

where

$$T_{b5} = c_b \ln 2 \frac{\sigma_0}{\sqrt{F_2 F_1}}$$

$$T_{s5} = c_s \ln 2 \frac{\sigma_0}{\sqrt{F_2 F_1}} - 5 \frac{0.288\sigma_0}{\Lambda_E} \frac{(F_2 - F_1)}{2F_1 F_2}$$

[68] The total load sediment flux in the basic state only has an alongshore component and consists of contributions caused by bed load and suspended load, given by:

$$q_{b0} \equiv \vec{q}_{b0,y} = \frac{3}{2}\nu_b u_w^2 V \quad q_{s0} \equiv \vec{q}_{s0,y} = \frac{32}{5\pi}\delta_m \hat{E}_{m,u} u_w^5 HV$$

The divergences of the perturbed sediment fluxes are

$$\vec{\nabla}\cdot\vec{q}_b' = \frac{3}{2}\nu_b \left\{ u_w^2 \left[\left(\frac{2}{u_w}\frac{\partial u_w}{\partial x} - \frac{1}{H}\frac{\partial H}{\partial x} \right) u' + \frac{V}{H}\frac{\partial h}{\partial y} \right] - \frac{8}{9\pi}\lambda_b u_w^3 \left(\frac{\partial^2 h}{\partial x^2} + \frac{3}{u_w}\frac{\partial u_w}{\partial x}\frac{\partial h}{\partial x} + \frac{\partial^2 h}{\partial y^2} \right) \right\}$$

$$\vec{\nabla}\cdot\vec{q}_s' = \frac{32}{5\pi}\delta_m \hat{E}_{m,u} \left\{ 5u_w^4 H \frac{\partial u_w}{\partial x} u' - \frac{\lambda_s}{7} u_w^7 H \left[\frac{\partial^2 h}{\partial x^2} + \left(\frac{7}{u_w}\frac{\partial u_w}{\partial x} + \frac{1}{H}\frac{\partial H}{\partial x} \right) \frac{\partial h}{\partial x} + \frac{\partial^2 h}{\partial y^2} \right] \right\}$$

Here, (18) has been used to eliminate v'.

Notation

c_b exponent in bed load transport capacity function
c_s exponent in suspended load transport capacity function
C_i depth-integrated volume concentration of grain sizes in class d_i, m
d_1 grain diameter of finest sediment fraction, mm
d_2 grain diameter of coarsest sediment fraction, mm
d_m mean grain size of a sediment mixture, mm
E_i entrainment of sediment of diameter d_i in suspension
$E_{i,u}$ as E_i, but in the case of uniform sediment
$\mathcal{F}_i$ probability distribution function for size class i in the active layer
F_i weight percent of the grains in the finest (i = 1) or coarsest (i = 2) grain size class in basic state
f_i perturbation on F_i (i = 1, 2)
$\mathcal{F}_s$ probability density function in substrate
$\mathcal{G}_{bi}$ bed load transport capacity function for sediment of size d_i
G_{bi} basic state bed load transport capacity function
g_{bi} perturbation on G_{bi}
$\mathcal{G}_{si}$ suspended load transport capacity function for sediment of size d_i
G_{si} basic state suspended load transport capacity function
g_{si} perturbation on G_{si}
L_a active layer thickness, m
L_{a0} basic state active layer thickness, m
m exponent in wave stirring function
m_b exponent in hiding function bed load
m_E exponent in entrainment of sediment in suspension
$\vec{q}_i$ total sediment flux of sediment of grain size d_i, including pores, m^2 s^{-1}
$\vec{q}_{bi}$ bed load flux of grains d_i, m^2 s^{-1}
q_{b0} basic state alongshore bed load flux, m^2 s^{-1}
$\vec{q}_b'$ perturbation in bed load flux, m^2 s^{-1}
$\vec{q}_{si}'$ suspended load flux of grains d_i, m^2 s^{-1}
q_{s0} basic state alongshore suspended load flux, m^2 s^{-1}
$\vec{q}_s'$ perturbation in suspended load flux, m^2 s^{-1}
u_w wave-orbital velocity amplitude, m s^{-1}
$\hat{u}_w$ near-bed wave-orbital velocity, m s^{-1}
δ_i ratio of the thickness of the suspended load layer of grains of diameter d_i over the total water depth
δ_m ratio of the thickness of the suspended load layer of grains of diameter d_m over the total water depth
ζ_i hiding function for entrainment of sediment in suspension
$\Theta_{i,u}$ Shields parameter for uniform sediment of size d_i
Θ_m Shields parameter for sediment of size d_m
λ_E straining parameter
Λ_E basic state straining parameter
λ_E' perturbation on Λ_E
ξ_i dynamic hiding function for bed load
σ standard deviation of the mixture on the phi scale
σ_0 standard deviation of the mixture in the basic state
σ' perturbation on σ_0
τ bed shear stress (skin friction), N m^{-2}
$\vec{\tau}_b$ bed shear stress vector (form drag + skin friction), N m^{-2}
ϕ_m mean grain diameter on phi scale
Φ_m basic state mean grain diameter
ϕ_m' perturbation on Φ_m

[70] **Acknowledgments.** This research was financially supported by the Cornelis Lely Foundation and the National Institute of Coastal and Marine Management in Netherlands (RIKZ) and by the EC-MAST 5 HUMOR project (contract EVK3-CT-2000-00037).

References

Admiraal, D. M., M. H. Garcia, and J. F. Rodriguez, Entrainment response of bed sediment to time-varying flow, *Water Resour. Res.*, *36*, 335–348, 2000.

Antia, E. E., Surficial grain-size statistical parameters of a North Sea shoreface-connected ridge: Patterns and process implication, *Geo Mar. Lett.*, *13*, 172–181, 1993.

Antia, E. E., Shoreface-connected ridges in German and US Mid-Atlantic bights: Similarities and contrasts, *J. Coastal Res.*, *12*, 141–146, 1996.

Bailard, J., An energetics total load sediment transport model for a plane sloping beach, *J. Geophys. Res.*, *86*, 10,938–10,954, 1981.

Bayram, A., M. Larson, H. C. Miller, and N. C. Kraus, Cross-shore distribution of longshore sediment transport: Comparison between predictive formulas and field measurements, *Coastal Eng.*, *44*, 79–99, 2001.

Calvete, D., M. Walgreen, H. E. De Swart, and A. Falqués, A model for sand ridges on the shelf: Effect of tidal and steady currents, *J. Geophys. Res.*, *106*, 9311–9326, 2001a.

Calvete, D., A. Falqués, H. E. De Swart, and M. Walgreen, Modelling the formation of shoreface-connected sand ridges on storm dominated inner shelves, *J. Fluid Mech.*, *441*, 169–193, 2001b.

Dyer, K. R., *Coastal and Estuarine Sediment Dynamics*, John Wiley, New York, 1986.

Figueiredo, J. A. G., J. E. Sanders, and D. J. P. Swift, Storm-graded layers on inner continental shelves: Examples from southern Brazil and the Atlantic coast of the central United States, *Sediment. Geol.*, *31*, 171–190, 1982.

Foti, E., and P. Blondeaux, Sea ripple formation: The heterogenous sediment case, *Coastal Eng.*, *25*, 237–253, 1995.

Fredsøe, J., and R. Deigaard, *Mechanics of Coastal Sediment Transport*, World Sci., River Edge, N. J., 1992.

Garcia, M., and G. Parker, Entrainment of bed sediment into suspension, *J. Hydraul. Eng.*, *117*, 414–435, 1991.

Green, M. O., C. E. Vincent, I. N. McCave, R. R. Dickson, J. M. Rees, and N. D. Pearson, Storm sediment transport: Observations from the British North Sea shelf, *Cont. Shelf Res.*, *15*, 889–912, 1995.

Hoogendoorn, E. L., Morphology, lateral migration, and internal structures of shoreface-connected ridges, Sable Island Bank, Nova Scotia, Canada, *Geology*, *14*, 400–403, 1986.

Lanzoni, S., and M. Tubino, Grain sorting and bar instability, *J. Fluid Mech.*, *393*, 149–174, 1999.

Lentz, S., R. T. Guza, S. Elgar, F. Feddersen, and T. H. C. Herbers, Momentum balances on the North Carolina inner shelf, *J. Geophys. Res.*, *104*, 18,205–18,226, 1999.

Niedoroda, A. W., and D. J. P. Swift, Maintenance of the shoreface by wave orbital currents and mean flow: Observations from the Long Island coast, *Geophys. Res. Lett.*, *8*, 337–340, 1981.

Parker, G., N. W. Lanfredi, and D. J. P. Swift, Seafloor response to flow in a Southern Hemisphere sand-ridge field: Argentine inner shelf, *Sediment. Geol.*, *33*, 195–216, 1982.

Ribberink, J. S., Mathematical modelling of one-dimensional morphological changes in rivers with non-uniform sediment, Ph.D. thesis, Tech. Univ. Delft, Netherlands, 1987.

Schwab, W. C., E. R. Thieler, J. R. Allen, D. S. Foster, B. A. Swift, and J. F. Denny, Influence of inner-continental shelf geologic framework on the evolution and behavior of the barrier-island system between Fire Island Inlet and Shinnecock Inlet, Long Island, New York, *J. Coastal Res.*, *16*, 408–422, 2000.

Seminara, G., Effect of grain sorting on the formation of bedforms, *Appl. Mech. Rev.*, *48*, 549–563, 1995.

Soulsby, *Dynamics of Marine Sands*, Thomas Telford, London, 1997.

Swift, D. J. P., and M. E. Field, Evolution of a classic sand ridge field: Maryland sector, North American inner shelf, *Sedimentology*, *28*, 461–482, 1981.

Swift, D. J. P., B. Holliday, N. Avignone, and G. Shideler, Anatomy of a shoreface ridge system, False Cape, Virginia, *Mar. Geol.*, *12*, 59–84, 1972.

Swift, D. J. P., G. Parker, N. W. Lanfredi, G. Perillo, and K. Figge, Shoreface-connected sand ridges on American and European shelves: A comparison, *Estuarine Coastal Mar. Sci.*, *7*, 257–273, 1978.

Trowbridge, J. H., A mechanism for the formation and maintenance of the shore-oblique sand ridges on storm-dominated shelves, *J. Geophys. Res.*, *100*, 16,071–16,086, 1995.

Van de Meene, J. W. H., and L. C. Van Rijn, The shoreface-connected ridges along the central Dutch coast, part 1, Field observations, *Cont. Shelf Res.*, *20*, 2295–2323, 2000.

Van de Meene, J. W. H., J. R. Boersma, and J. H. J. Terwindt, Sedimentary structures of combined flow deposits from the shoreface-connected ridges along the central Dutch coast, *Mar. Geol.*, *131*, 151–175, 1996.

Van Rijn, L. C., *Principles of Sediment Transport in Rivers, Estuaries and Coastal Seas*, Aqua Publ., Amsterdam, 1993.

Zyserman, J. A., and J. Fredsøe, Data analysis of bed concentrations of suspended sediment, *J. Hydraul. Eng.*, *120*, 1021–1042, 1994.

H. E. de Swart and M. Walgreen, Institute for Marine and Atmospheric Research (IMAU), Utrecht University, Princetonplein 5, NL-3584 CC, Utrecht, Netherlands. (M.Walgreen@phys.uu.nl)

D. Calvete, Department de Física Applicada, Universitat Politècnica de Catalunya, E-08034 Barcelona, Spain.